Research Square

Preprints are preliminary reports that have not undergone peer review.
They should not be considered conclusive, used to inform clinical practice,
or referenced by the media as validated information.

Construction of prognostic features associated with the tumor microenvironment and endothelial cells in cervical cancer by combining single-cell and transcriptomic data and PCR validation

Yinzhuoyang A
The First People's Hospital of Yunnan Province
Dongyan Ren
The First People's Hospital of Yunnan Province
Yulin Zhang
Kunming University of Science and Technology
Tao Yu
The First People's Hospital of Yunnan Province
Guoqiao Zhang
zgqnhm@sina.com

The First People's Hospital of Yunnan Province

Research Article

Keywords: cervical cancer, prognostic genes, tumour ecosystems, endothelial cells, PCR

Posted Date: March 23rd, 2026

DOI: https://doi.org/10.21203/rs.3.rs-8884166/v1

License: This work is licensed under a Creative Commons Attribution 4.0 International License.
Read Full License

Additional Declarations: No competing interests reported.

Construction of prognostic features associated with the tumor microenvironment and endothelial cells in cervical cancer by combining single-cell and transcriptomic data and PCR validation

Yinzhuoyang A1,3, Dongyan Ren2,3, Yulin Zhang4, Tao Yu2,3*, Guoqiao Zhang1,3*

1Department of Medical Oncology,The First People's Hospital of Yunnan Province, Kunming, China

2Department of Gynecology, The First People's Hospital of Yunnan Province, Kunming, China

3Kunming University of Science and Technology Affiliated Hospital, Kunming, China

4School of Medicine, Kunming University of Science and Technology, Kunming, China

*** Correspondence:**

Guoqiao Zhang

zgqnhm@sina.com, No. 157, Jinbi Road, Xishan District, Kunming City, Yunnan Province, China, +8615198809539

ORCID

https://orcid.org/0009-0005-0049-4674

Acknowledgments

We would like to express our sincere gratitude to all individuals,Yunnan revitalization talent support program and Beijing Science and Technology Medical Development Foundationorganizations who supported and assisted us throughout this research. Special thanks to the following authors: Guoqiao Zhang, Tao Yu,Yinzhuoyang A. In conclusion, we extend our thanks to everyone who has supported and assisted us along the way. Without your support, this research would not have been possible.

Author contributions

All authors contributed to the study conception and design. Material preparation, data collection and analysis were performed by [Yinzhuoyang A], [Dongyan Ren] and [Yulin Zhang]. The first draft of the manuscript was written by [Yinzhuoyang A] and all authors commented on previous versions of the manuscript. All authors read and approved the final manuscript.

Clinical trial number: not applicable.

Abstract

Cervical cancer (CC) ranks among the most common gynecological malignancies. This study aimed to investigate the prognostic value of genes associated with tumor ecosystem (TES) and endothelial cells in CC. Key cells were identified through the analysis of single-cell RNA sequencing (scRNA-seq) data. Differentially expressed genes (DEGs) associated with TES were intersected with marker genes associated with key cells to identify candidate genes. Prognostic genes were selected through analyses such as univariate regression and machine learning. A nomogram was constructed and validated. Immune cell infiltration profiles were assessed using the CIBERSORT algorithm. scRNA-seq analysis identified endothelial cells as key cells. The intersection of marker genes associated with key cells and DEGs associated with TES yielded 17 candidate genes. Five prognostic genes (ALKBH2, CXCL1, TFPI2, PLAU, and CXCL8) were identified through analyses such as machine learning algorithms. A nomogram model exhibited high sensitivity and specificity. Immune infiltration analysis identified 7 types of differential immune cells, including plasma B cells, Macrophage M0, activated mast cells, resting myeloid dendritic cells, and others. These findings collectively provided novel insights into the molecular mechanisms and immune microenvironment characteristics underlying TES, laying a foundation for the development of potential therapeutic targets and prognostic biomarkers.

Keywords: cervical cancer, prognostic genes, tumour ecosystems, endothelial cells, PCR

1. Introduction

Cervical cancer (CC) ranks as the fourth most common cancer among women worldwide, both in terms of incidence and mortality. According to the 2020 Global Cancer Statistics, there are approximately 600,000 new cases and 340,000 deaths annually, with these numbers showing a consistent upward trend [1].Persistent infection with high-risk human papillomavirus (HPV), especially types 16 and 18, is a major risk factor for CC, although it is not the only factor. Other high-risk factors include young age of first sexual intercourse, multiple sexual partners, early childbearing, multiple pregnancies, smoking, and having sexually transmitted diseases, etc [2]. While preventive HPV vaccines are now globally available, their accessibility remains limited in many developing countries due to severe shortages of medical resources [3].This has led to women in developing countries being continuously exposed to the risk of HPV infection, thereby making it difficult to effectively control the incidence of CC and keeping it at a relatively high level continuously. Despite advances in treatment strategies, including a multidisciplinary approach combining surgery, radiotherapy, and chemotherapy, the prognosis for CC patients remains suboptimal, with approximately 75% of patients experiencing disease progression or recurrence [4]. Especially for locally advanced or metastatic CC, surgery is complicated to remove cancer cells [5]. Moreover, treatment-related complications significantly compromise patient quality of life (QoL). Radiation therapy frequently leads to adverse effects including radiation enteritis, cystitis, ovarian dysfunction, and vaginal impairment [6], while chemotherapy commonly induces leukopenia, nephrotoxicity, and neurotoxicity [7].This persistent clinical challenge underscores the urgent need for more effective therapeutic interventions and improved prognostic tools.

Increasing evidence suggests that tumor heterogeneity extends beyond tumor cells to encompass the broader tumor ecosystem (TES). This ecosystem comprises a matrix of non-tumor cells, including fibroblasts, inflammatory cells, and blood vessels, contributing to tumor progression [8]. These cells produce cytokines, growth factors, and extracellular matrix proteins while providing essential nutrients to support tumor cell survival and invasion [9]. Together, they create a dynamic microenvironment that facilitates tumor growth, invasion, and metastasis. The heterogeneity of this complex TES plays a critical role in the initiation, malignant progression, and treatment response of CC [10]. Angiogenesis is crucial in both normal and cancerous tissues, making it a key therapeutic target. Research shows tumor-derived endothelial cells (TECs) differ significantly from normal endothelial cells (NECs), exhibiting enhanced proteolytic activity and metabolic reprogramming to support tumor growth [11]. While NECs primarily regulate basic vascular functions, TECs activate tumor-specific pathways including PPAR signaling, amino acid biosynthesis, glycolysis, and cell cycle regulation [12]. These distinct features highlight TECs' role in tumor progression and reveal potential targets for anti-angiogenic therapies.

Advances in single-cell RNA sequencing (scRNA-seq) technology have enabled researchers to dissect tumor heterogeneity at an unprecedented resolution. By analyzing gene expression profiles at the single-cell level, scRNA-seq reveals the distribution and functional states of diverse cell populations within tumors [13]. This approach has provided insights into intratumoral heterogeneity, dynamic changes in cell states during tumor evolution, and the identification of functional biomarkers. It also offers a deeper understanding of individual differences in treatment response [14,15]. In the context of CC, scRNA-seq studies have elucidated the transcriptional profiles of both normal and tumor cells, highlighting the heterogeneity of tumors and their microenvironments [16]. These studies have characterized the features of the CC tumor microenvironment (TME) across various stages, from precancerous lesions to invasive tumors and metastatic lymph nodes. However, the mechanisms by which this heterogeneity drives CC progression and confers treatment resistance remain poorly understood. Further research is needed to unravel these complex interactions and identify potential therapeutic targets [17].

Based on transcriptomic data and single-cell data from public databases, this study screened for candidate genes related to the CC TES and endothelial cells and then constructed a related risk model. It further analyzed the differences in immune characteristics and the relationship between prognostic genes in high- and low-risk groups. The differences in responses to immunotherapy and drug treatment between the two groups of patients were also compared.

2. Materials and methods

2.1 Data collection

The data related to CC were acquired from the Cancer Genome Atlas (TCGA) and GEO database. A total of 293 samples containing survival information were obtained from TCGA-CC dataset and then, they were randomly divided into a training set containing 206 samples and a validation set containing 87 samples. Tumour samples from 76 CC patients and 24 normal control samples were obtained from the dataset of GSE63514 (GPL570). Tumour samples from 33 CC patients and 24 normal control samples were obtained from the dataset of GSE9750 (GPL96). Tumour samples from 3 CC patients and 2 normal control samples were obtained from the single-cell dataset of E-MTAB-11948 from the European Molecular Biology Laboratory's European Bioinformatics Institute (EMBL-EBI) database. Additionally, 2,434 TES-related genes (TES-RGs) were obtained from the published literature [9].

2.2 Identification of differentially expressed genes (DEGs)

DEGs with thresholds of "|log2fold-change (FC)| > 1 and $p < 0.05$", between the CC and the control samples of GSE63514 were identified by the "limma" package (v 3.54.0) [18]. DEGs were ranked according to the log2FC, and then top 10 up-

regulated and top 10 down-regulated were displayed. The results were visualised using the "ggplot2" packages (v 3.4.1) [19] and "complexHeatmap" (v 2.14.0) [20].

2.3 Acquisition of "DEGs associated with TES" and functional enrichment analysis

To investigate the biological pathways and signaling pathways involved in TES-related DEGs, we performed kyoto encyclopedia of genes and genomes (KEGG) pathway analysis and gene ontology (GO) functional enrichment analysis on the candidate genes using the "ClusterProfiler" package (v 4.7.1.003) (PMID: 34557778) . Among them, the GO analysis covered three components: biological process (BP), cellular component (CC), and molecular function (MF), with a significance threshold set at $p < 0.05$.

2.4 Single-cell RNA sequencing (scRNA-seq) data processing

The scRNA-seq data was processed by "Seurat" package (v 4.1.0) [21]. In order to obtain high-quality data, we filtered the raw data using the "Create Seurat Object" function. Cells with a gene count of less than 200 but greater than 6,000, cells with read counts greater than 30,000, and cells with more than 20% of mitochondrial genes were excluded. We used the "Find Variable Features" function to select genes with a high degree of variability. The results were visualized with the "LabelPoints" function. The samples were normalized using the "Scale Data" function. Principal component analysis (PCA) was performed through the "RunPCA" function, and the statistically significant principal components ($p < 0.05$) were screened using the "jackstrawplot" function. Unsupervised cluster analysis of cells was performed to obtain different cell clusters with thresholds of "resolution = 1.2" using "FindNeighbors" and "FindClusters" functions, and the results were visualized by the UMAP algorithm. The clusters were further classified into different cell types according to marker genes in the published literature [22,23].

Furthermore, the functional enrichment of cell types was analyzed using "analyze_sc_clusters" functions of R package "ReactomeGSA" (v 1.16.1) [24]. The proportion differences of different cell types between CC and control samples were analyzed to obtain key cells by Fisher's test. The differential analysis of key cells was conducted to obtain "marker genes related to key cells" using the "FindMarkers" function, and the threshold was "|average log2FC| > 1 and $p < 0.05$". The results were visualized by "Manhattan Plot". Then, "marker genes related to key cells" were crossed with "DEGs associated with TES" to obtain candidate genes via the R package "VennDiagram" (v 1.7.3) [25].

2.5 Construction and validation of a risk model and construction of nomogram

In the TCGA-CC cohort, the univariate Cox regression model with the threshold of "Hazard Ratio (HR)" ≠ 1 (95% CI) and $p < 0.05$" was performed to obtain genes with prognostic value by the "survival" package (v 3.5.3) [26]. The proportional hazards (PH) hypothesis test was executed to ensure the reliability of univariate Cox regression via the "Cox.zph" function.

Least absolute shrinkage and selection operator (LASSO) regression was performed via the "glmnet" package (v 4.1.4) [27]. In the training set, the prognostic genes were used for constructing the following model:

$$\text{risk score}=\sum_{i=1}^{n}\text{coef}(\text{gene}_i)\times\text{expr}(\text{gene}_i)$$

Then, samples in the training set were divided into high-risk group (HRG) and low-risk group (LRG). Kaplan-Meier (K-M) curves were plotted to compare the difference of survival between the HRG and LRG via "survminer" package (v 0.4.9) [28]. Receiver operating characteristic (ROC) curves were plotted to evaluate the accuracy of the risk model predictions via the R package "survivalROC" (v 1.0.3) [29]. Finally, the robustness of the risk model was verified in the validation set. Nomograms were constructed based on prognostic genes by the "rms"package (v 6.5.0) [30], and the accuracy of nomograms was evaluated by calibration curve. The predictive performance of the nomogram model was evaluated by plotting ROC curves using the "pROC" package (v 1.18.0) [31].

2.6 Gene set variation analysis (GSVA)

The GSVA had been carried out using the "GSVA" package (v 1.42.0) [32]. "h.all.v2023.1.Hs.symbols.gmt" was used as reference gene set. The GSVA scores of HRG and LRG samples in TCGA-CC dataset were calculated, and then the difference of GSVA scores was analyzed using the "limma" package (v 3.54.0) [18]. Differential pathways between the two groups were selected according to the threshold of "$p < 0.05$".

2.7 Immune infiltration landscape

The proportion of immune cell infiltration in HRG and LRG in TCGA-CC dataset was calculated by CIBERSORT, XCELL, and TIMER algorithm. Differences in immune cell infiltration fraction, immune related functions, and immune checkpoints were analyzed by the Wilcoxon test [33]. Correlations between prognostic genes and differential immune cells, as well as between prognostic genes and differential immune checkpoints were calculated using the R package "psych" (v 2.2.9) [34]. The threshold was "$| r | \geq 0.3$ and $p < 0.05$".

2.8 Pseudotime analysis and cellular communication network

To investigate the evolutionary trajectory of key cells, pseudotime analyses were performed in E-MTAB-11948 dataset using the R package "Monole2" (v 2.22.0). Gene dynamics during cell differentiation were explored through "DiffialGeneTest" functions. Cell communication was analysed through the "CellPhoneDB" package (v 1.5.0) [35].

2.9 Immunotherapy and drug sensitivity analysis

Next, we analyzed the sensitivity differences of the two groups of patients from TCGA-CC dataset in response to immunotherapy and drug treatment. Immunophenotype scores (IPS) of CC patients were obtained from the TCIA

database, and then IPS of two groups of patients were calculated to evaluate the immunotherapeutic effects by Wilcoxon test. Half-maximal inhibitory concentration (IC50) values of 198 common chemotherapeutic drugs were calculated for all patients using the R package "pRRophetic" (v 0.5) [36]. The difference of IC50 values between HRG and LRG was further analyzed using the Wilcoxon test.

2.10 Experimental validation of prognostic genes

From September to December in 2024, this study collected 5 pairs of cervical cancer tissue and corresponding adjacent tissue samples from the First People's Hospital of Yunnan Province, and detected the expression of prognostic genes using real-time quantitative polymerase chain reaction (RT-qPCR) technology. Briefly, RT-qPCR was performed using S1000 ™ Thermal Cycler ordinary PCR instrument and CFX Connect real-time quantitative fluorescence PCR instrument (BIO-RAD). TRizol reagent was used for total RNA extraction of tumor tissue sample. Hifair®III 1st Strand cDNA synthesis supermix for qPCR was used to synthesize complementary DNA (cDNA). Each RT-qPCR reaction system was composed of 3μL cDNA, 5μL 2xUniversal Blue SYBR Green qPCR Master Mix, 1μL forward primer and 1μL reverse primer. Next, we used $2^{-\Delta\Delta CT}$ method to calculate the relevant gene expression. Primer details were displayed in **Online Resource 1**. There were 2 groups including CC group and control group, and each group had five samples. Three biological replicates were established in total. The differences of expression between the two groups were analyzed using t-test. $P < 0.05$ was considered statistically significant.

2.11 Statistical analysis

Bioinformatic analysis was carried out using the R language (v 4.2.2). The Wilcoxon test was used to analyze the differences between groups. $P < 0.05$ was considered to be statistically significant.

3. Results

3.1 Identification and functional enrichment analysis of DEGs associated with TES

A total of 3,272 DEGs (2,348 up-regulated and 924 down-regulated genes) were identified between CC and control samples in GSE63514 dataset (**Fig. 1a-b**). And then 3,272 DEGs and 2,434 TES-RGs were crossed to obtain 607 "DEGs associated with TES" (**Fig. 1c**). Then, the biological functions of these genes were explored, and the results showed that the GO entries, which included 232 biological processes (BPs), 40 cellular components (CCs), and 53 molecular functions (MFs), were involved in multiple aspects (**Online Resource 2**). In detail, the top 3 items enriched of BPs included "vesicle-mediated transport in synapse". The top 3 items enriched of CCs were "axon terminus". The top 3 items enriched of MFs were "ligand-gated monoatomic cation channel activity" (**Fig. 1d**). Meanwhile, 11 KEGG pathways indicated that 607 DEGs associated with TES were found to be significantly correlated with hormone regulation, for instance, "insulin secretion"

and “adrenergic signaling in cardiomyocytes” (**Fig. 1e and Online Resource 3**).

3.2 Analysis of single-cell transcriptome data and identification of key cells

Single-cell sequencing is an effective method that could accurately reveal organisational heterogeneity and assess gene expression at the cellular level39. The gene count, gene expression count, and percentage of mitochondrial genes before and after the removal of low-quality cells were shown in **Fig. 2a-b**. Ultimately, a total of 51,324 cells and 27,370 genes were included in further analysis. Then, we selected 2,000 genes that were highly variable, and the top 10 including *SCGB3A1*, *IGKC*, and *IGHG1* were labeled (**Fig. 2c**). Additionally, 20 principal components were obtained through PCA (**Fig. 2d-e**). Then, the cells were subjected to unsupervised clustering and divided into 21 cell clusters as shown in Fig. 2f. Then, these cell clusters were further classified, resulting in 8 cell types (endothelial cells, macrophage, fibroblasts, smooth muscle cells, neutrophils, epithelial or cancer cells, T cells, and B cell) (**Fig. 2g**), and the marker genes for these 8 cell types were shown in **Fig. 2h**.

Then, the biological functions of these cell types showed that a total of 1,782 pathways were enriched, involving various aspects, such as “alanine metabolism related to metabolism”, “interleukin-6 signaling” and “antigen processing cross presentation” related to immunity, and “neurotransmitter release cycle” related to substance transport (**Online Resource 4 and Online Resource 5**).

Furthermore, to obtain endothelial cells, the expression differences of 8 cell types between CC and control samples were analyzed, and Fisher's test showed that there were significant differences in 8 cell types (**Table. 1**). Additionally, relevant reports indicated that vascular endothelial cells were a key target for CC treatment12. Therefore, endothelial cells were selected as endothelial cells for subsequent analysis.

3.3 Identification of candidate genes and construction of risk model related to TES and endothelial cells

Firstly, we conducted a differential analysis of endothelial cells between the CC group and the control group, and the results showed that there were 222 genes with differences between the endothelial cells of the two groups (**Fig. 3a**). Then, these 222 genes were defined as “marker genes related to endothelial cells” and they were crossed with 607 “DEGs associated with TES” to obtain 17 candidate genes (**Fig. 3b**).

Next, the result of univariate Cox regression analysis showed 6 candidate genes (*ALKBH2*, *ISG20*, *CXCL1*, *TFPI2*, *PLAU*, and *CXCL8*) were significantly associated with prognosis (**Fig. 3c**). Moreover, *CXCL1*, *TFPI2*, *PLAU*, and *CXCL8* had *HR* greater than 1, suggesting that they were risk factors for CC. Conversely, the HRs of *ALKBH2* and *ISG20* were less than 1, implying that they were protective factors for CC. Furthermore, the results of the PH hypothesis test indicated that *ALKBH2*, *CXCL1*, *TFPI2*, *PLAU*, and *CXCL8* were relatively reliable in univariate Cox regression analysis (**Table 2**). The LASSO

regression analysis indicated that when the optimal lambda value was 0.0121556, the model was considered to have the smallest residual sum of squares (**Fig. 3d-e**). At this time, a total of 4 prognostic genes (*ALKBH2*, *TFPI2*, *PLAU*, and *CXCL8*) were obtained and used to construct a risk model in relation to TES and endothelial cells. Risk score = -0.35 × *ALKBH2* + 0.07 × *TFPI2* + 0.14 × *PLAU* + 0.20 × *CXCL8*. Then, samples in the training set had been divided into HRG and LRG on the basis of the cutoff value (0.8512157) (**Fig. 3f**). Moreover, the number of deaths gradually increased with increasing risk scores (**Fig. 3g**). *PLAU*, *CXCL8*, and *TFRI2* were more highly expressed in the HRG, while *ALKBH2* had the opposite result (**Fig. 3h**). Patients in the HRG had a worse chance of survival than those in the LRG ($p < 0.0001$, **Fig. 3i**). The ROC curves indicated that the risk model could make good predictions for the survival of CC patients (the value of AUC for 1-year, 3-years, and 5-years = 0.73, 0.69, and 0.72) (**Fig. 3j**).

Furthermore, we validated the robustness of the risk model in the validation set. The distribution of risk score, survival status of patients, and expression of prognostic genes between HRG and LRG were shown in the **Fig. 4a-c**. Additionally, patients in the HRG had a worse chance of survival than those in the LRG ($p = 0.0023$) (**Fig. 4d**). The risk score showed superiority in predicting the survival of CC (AUC > 0.7) (**Fig. 4e**). In summary, the risk model in relation to TES and endothelial cells had a certain degree of robustness in predicting the survival of CC in different years。

3.4 Construction of prognostic nomogram and analysis of differential pathways between HRG and LRG groups

In order to construct an effective tool for predicting survival, a nomogram model was constructed on the basis of prognostic genes (**Fig. 5a**). In the calibration curve, the slope was close to 1, indicating that the true predictive performance of the nomogram was close to the ideal model (**Fig. 5b**). The values of AUC for predicting overall survival of CC patients were greater than 0.6 (**Fig. 5c**). In conclusion, the nomogram model had a good predictive effect on the survival of CC patients.

GSVA is an advantageous method for analyzing biological differences between different groups. There were 6 pathways with differences between HRG and LRG (**Fig. 5d**). “Spermatogenesis” and “oxidative phosphorylation” were suppressed in the HRG. “TNFA signaling via NFKB” and “angiogenesis” were activated in the HRG (**Fig. 5e**).

3.5 Landscape of immune cell infiltration

Landscape of immune cell infiltration between HRG and LRG was shown in **Fig. 6a.** In detail, 7 kinds of cells including “B cell plasma”, “macrophage M0”, and “activated mast cell” had significantly differential infiltration score between the two groups (**Fig. 6b**). Then, the correlation between these differential cells and 4 prognostic genes was further analysed, and we found that *CXCL8* was correlated with “activated mast cell” (r = -0.37) (**Fig. 6c**). In addition, **Fig. 6d** demonstrated the differences of immune-related functions between the HRG and LRG, and we could find that chemokine receptor (CCR) and human leukocyte antigen (HLA) were significantly different between both groups (**Fig. 6e**). There were statistically

significant differences in the expression of 9 immune checkpoints (CD276, CD44, LAG3, PDCD1, PDCD1LG2, TIGIT, TNFRSF18, TNFRSF25, and VTCN1) between HRG and LRG (**Fig. 6f**). Among them, *PLAU* was correlated with CD44 (r = 0.46), and *CXCL8* was positively correlated with CD276 (r = 0.30) (Fig. 6G and **Online Resource 6**).

In addition, we further analyzed the immune cell infiltration landscape of CC using different algorithms. Specifically, the result of TIMER algorithm indicated that the infiltration scores of immune cells were significantly different between HRG and LRG (**Online Resource 7 and Online Resource 8**). Moreover, *CXCL8* was negatively correlated with "T cell CD4+" and "macrophage", while *PLAU* was positively correlated with "neutrophil" ($|r| > 0.3$) (**Online Resource 9 and Online Resource 10**). The results of XCELL algorithm showed that a total of 10 cell infiltration scores, including "B-cells", "epithelial cells", and "neutrophils", were significantly different (**Online Resource 11 and Online Resource 12**). Moreover, *CXCL8* showed significant correlation with four types of cells. *ALKBH2* showed significant correlation with "naive CD8 T cells" and "pro B cells" ($|r| > 0.3$) (**Online Resource 13 and Online Resource 14**)

3.6 Evolutionary trajectory and cellular communication analysis of endothelial cells

Next, in order to investigate the evolutionary trajectory of endothelial cells, pseudotime analysis was conducted. Specifically, the epithelial cells were re-clustered into 9 subgroups. Then we combined cells of different subtypes with pseudo temporal trajectories to reveal the developmental status of different subgroups. It turned out that subgroup 2 had the earliest developmental time and subgroup 7 had the latest developmental time, in other words, subgroup 7 took longer to develop than subgroup 2 (**Fig. 7a-b**). Then, we analysed the trend of prognostic genes' expression during endothelial cell development, and the results revealed that *ALKBH2* tended to increase, then decrease, then stabilise. The expression of *TFPI2* and *CXCL8* tended to increase, then decrease, then increase. *PLAU* tended to decrease, then stabilise, then increase **(Fig. 7c**).

The results of the cellular communication network implied that in the control group, endothelial cells had the highest number of interactions with other cells (**Fig. 7d**) and, moreover, the strength of interactions was the highest between endothelial cells and neutrophils (**Fig. 7e**), and the same results were found in the CC group (**Fig. 7f-g**).

3.7 Immunotherapy and drug treatment responses

The correlation between prognostic genes and immune infiltration implied that immunotherapy could play a potential role in treating CC. To evaluate the response of two groups of patients to anti-PD1 and anti-CTLA4 immunotherapy, we calculated the IPS of two groups of patients. The results showed that in the immunotherapy of "anti-IPS-CTLA4" and "anti-IPS-CTLA4 and PD1/PDL1/PDL2", the two groups of samples exhibited different therapeutic effects (**Fig. 8a**). The sensitivity results of chemotherapy drugs showed that a total of 66 drugs, including "axitinib1021",

"dihydrorotenone_1827", and "GSK269962_1192", showed differences between the HRG and LRG (**Fig. 8b**).

3.8 Expression analysis of prognostic genes

In addition, in the GSE63514 dataset, the expression levels of prognostic genes (*ALKBH2*, *PLAU*, and *CXCL8*) were significantly higher in CC samples compared to controls, while *TFPI2* was lower (**Fig. 9a**). In the GSE9750 dataset, compared to the control group, the expression of *PLAU* and *CXCL8* was increased in the CC group. However, the expression of *TFPI2* did not show significant differences between CC and controls. Moreover, *ALKBH2* was not found in the GSE9750 dataset (**Fig. 9b**). In addition, the expression of prognostic genes in low-, medium-, and high-grade CC samples was detected and we found that the expression of *ALKBH2* showed a gradual upward trend in the three groups of samples (**Fig. 9c**). The results of RT-qPCR showed that compared with adjacent tissues, the expression of *PLAU* and *CXCL8* was significantly increased in cancer tissues, while the expression of *TFPI2* was significantly decreased. In addition, there was no significant difference in the expression of *ALKBH2* between the two groups (**Fig. 9d**). In conclusion, the expression of *PLAU* and *CXCL8* showed consistency in the GEO analysis and in the validation of clinical samples.

4. Discussion

CC is one of the most common cancers in women. Despite the application of a multidisciplinary approach combining surgery, radiotherapy and chemotherapy in CC patients, the prognosis remains unsatisfactory, with approximately 75% of patients experiencing disease progression and recurrence4. An increasing number of studies have shown that tumor heterogeneity is reflected in tumor cells and the tumor ecosystem, the soil in which tumor cells grow [9]. Research shows TECs differ significantly from NECs, exhibiting enhanced proteolytic activity and metabolic reprogramming to support tumor growth [12]. This study identified 17 candidate genes related to tumor endothelial signature and endothelial cells from multiple datasets. A risk model was built using four prognostic genes (*ALKBH2*, *TFPI2*, *PLAU*, and *CXCL8*) and showed differences in immune cell infiltration, immune functions, and immune checkpoints between high-risk and low-risk groups. The prognostic gene *CXCL8* was correlated with specific immune cells and an immune checkpoint gene. The findings may offer a new perspective for CC's prognosis and immunotherapy strategies.

We identified four prognostic genes: *ALKBH2*, *TFPI2*, *PLAU*, and *CXCL8*. Extensive research indicates that these genes exhibit differential expression across various tumor types, including CC, and play distinct roles in tumorigenesis and progression. For example, *PLAU* is frequently overexpressed in multiple malignancies, such as head and neck squamous cell carcinoma, bladder urothelial carcinoma, and cholangiocarcinoma. It contributes to tumor progression by enhancing cancer cell proliferation, migration, invasion, and epithelial-mesenchymal transition (EMT) [37-39]. Furthermore, *PLAU* has been proposed as a potential prognostic biomarker for tumors [40]. In CC, *PLAU* drives CC progression by regulating

EMT (downregulating E-cadherin while upregulating MMP-9/Cyclin D1), as evidenced by inhibited proliferation, migration and invasion upon its knockdown in HeLa/HT3 cells [41]. Our analysis confirms *PLAU* overexpression in CC, supporting its potential as both a prognostic biomarker for disease severity and a promising therapeutic target.

CXCL8 is one of the most representative chemokines synthesized and secreted by malignant cells, endothelial cells and lymphocytes, and it is a potential target for therapeutic intervention in human diseases [42,43]. The study has demonstrated that *CXCL8* expression (mRNA and protein levels) was markedly elevated in CC tissues and cell lines compared to normal cervical and epithelial cell lines, clinically correlating with advanced disease stage, distant metastasis, histological subtype, and tumor grade, while emerging as an independent poor prognostic factor in CC patients [44]. Our PCR experiments also verified that the expression of *CXCL8* was significantly increased in cancer tissues.

In contrast, *TFPI2* is frequently downregulated in several cancer types, including prostate cancer, pancreatic ductal adenocarcinoma, gastric cancer, and non-small cell lung cancer [45-48]. Its downregulation has been associated with reduced survival rates in breast cancer patients and is known to exert anti-angiogenic effects [49,50]. In CC, research results show that *TFPI2* has a dual epigenetic inhibitory effect at the transcriptional level of promoter methylation in cancer cells and the translation level of miR-23a in tumor-associated fibroblasts, with its functional inactivation playing a pivotal role in disease progression [51]. This finding is consistent with the PCR verification result of our study that the expression of *TFPI2* in CC tissues is significantly reduced.

The ALKBH protein family, including *ALKBH2*, is highly expressed in various human malignancies [52,53]. For instance, research shows that *ALKBH2* promotes colorectal cancer progression by activating the BMI1/NF-κB pathway, and its suppression attenuates tumor malignancy, highlighting its therapeutic potential in CRC treatment [54]. So far, no studies related to *ALKBH2* and CC have been found. Our bioinformatics analysis suggested *ALKBH2* as a protective factor with higher expression in low-risk group. At the same time, PCR results paradoxically showed its elevated expression in CC tissues, particularly in high-grade cases. It is speculated that *ALKBH2* plays a dual regulatory role in cervical cancer: it exhibits tumor-suppressive activity in the early stages of the disease or in low-risk patients. However, during the progression of advanced-stage disease, it may exert a pro-tumor effect through interactions with the tumor microenvironment or the body's compensatory mechanisms. This dynamic change in expression and function may be attributed to the unique pathogenesis of cervical cancer or the imbalanced complex regulatory network caused by tumor heterogeneity.

In summary, these findings underscore the critical roles of *ALKBH2*, *TFPI2*, *PLAU*, and *CXCL8* in tumor biology, particularly in CC, and suggest their potential as prognostic markers and therapeutic targets.

Building on the four prognostic genes (*ALKBH2*, *TFPI2*, *PLAU*, and *CXCL8*), we developed a predictive model to estimate survival outcomes in CC patients and validated its effectiveness. This model adds to a growing body of literature exploring prognostic tools for CC. For instance, cancer-associated fibroblast-related features have been utilized to predict clinical outcomes and immune responses in CC [55]. At the same time, heat shock protein-related genes have been employed to forecast prognosis and immune landscape characteristics [56]. These diverse approaches to identifying prognostic factors highlight the complexity of tumorigenesis and progression and provide a foundation for uncovering potential therapeutic targets.

Our research found that 7 kinds of immune cells had significantly different infiltration scores between the high-risk group(HRG) and the low-risk group(LRG), among which the difference in “activated mast cells “was the most significant. Activated mast cells release various inflammatory mediators, including histamine [57]. Elevated histamine levels have been observed in multiple tumor types such as colorectal, breast, and skin cancers, and are closely associated with tumor growth and progression [58,59]. Studies have demonstrated that mast cells promote CC cell migration through mediator release, an effect that can be inhibited by modulating mast cell activation status or blocking relevant receptors [60]. In our study, the negative correlation between the prognostic gene *CXCL8* and activated mast cells suggests its potential role in suppressing mast cell activity or counteracting their pro-tumor effects within the tumor microenvironment. *CXCL8* may modulate tumor progression by regulating the balance of inflammatory mediators, thereby shifting the microenvironment toward an anti-inflammatory state. We identified the immune checkpoint CD276 (B7-H3) as significantly differentially expressed between high- and low-risk CC patient groups, correlating with the prognostic genes *CXCL8*, *TFPI2*, and *PLAU*. Anti-CD276 antibodies eliminate cancer stem cells (CSCs) via CD8+ T cells in head and neck squamous cell carcinoma （HNSCC） mouse models, suppressing tumor growth and lymph node metastasis. At the same time, scRNA-seq shows CD276 blockade reduces tumor heterogeneity and epithelial-mesenchymal transition (EMT), highlighting its immune evasion role and therapeutic potential [61]. Published studies also indicate that CD276 (B7-H3) expression promotes the secretion of IL-10 and TGF-β1, fostering an immunosuppressive microenvironment that drives CC progression. This process may be regulated by the p-JAK2/STAT3 signaling pathway [62]. Notably, CD276 expression is significantly higher in CC tissues than normal cervical tissues, and its overexpression is associated with poorer prognosis in CC patients [63]. In summary, these findings underscore the potential of CD276 (B7-H3) as a promising therapeutic target for CC, offering new avenues for immune-based interventions.

This study revealed significant differences in immunotherapy responses between low- and high-risk patient groups. low-risk patients have a higher degree of immune cell infiltration (such as "CD8+ T cell" and "regulatory T cell (Tregs)"),

stronger immune function (HLA), and better responses to anti-CTLA-4 and anti-CTLA-4 + PD1/PDL1/PDL2 treatments. These findings highlight the potential of risk stratification to guide personalized treatment strategies, particularly in the context of immunotherapy and targeted therapy for CC.

During our investigation into key cellular components, we observed significant differences in endothelial cells（EC） between CC and control samples ($p = 0$). NECs had essential biological functions, such as vascular system development, angiogenesis, EC migration, and endothelial development, in contrast, TECs exhibited significant enrichment in proteolytic regulation (peptidase activity modulation and extracellular matrix reorganization) and tumor-supportive metabolic pathways（xenobiotic metabolism, PPAR signaling, amino acid and carbon metabolism, and glycolytic processes, while additionally promoting tumor cell proliferation through activation of DNA replication, tricarboxylic acid cycle, and cell cycle regulation pathways, aligning with their tumor-promoting phenotype [12]. Our cellular communication analysis revealed that endothelial cells exhibited the strongest interaction intensity with neutrophils. Previous studies have demonstrated that endothelial cell migration is critical in various diseases characterized by excessive vascular proliferation, including cancers, arthritis, and atherosclerosis [64]. Immune cells serve as a reservoir for synthesizing and secreting bioactive factors that promote endothelial cell migration. Conversely, endothelial cells complete the migration process, which may promote the infiltration of neutrophil cells into the surrounding tissues [65]. Research indicates that neutrophil recruitment is likely mediated through the oxidized LDL/LOX-1 axis in tumor endothelial cells, and this process further contributes to the formation of a highly metastatic tumor microenvironment [66]. These findings reveal the multifaceted role of endothelial cells in cervical cancer. TECs directly promote tumor proliferation and survival through diverse metabolic and proliferative pathways, while their interaction with neutrophils modulates the immune microenvironment to facilitate tumor invasion and metastasis. These results highlight endothelial cells' complexity and therapeutic potential in the tumor microenvironment.

In conclusion, this study integrated multiple datasets, screened candidate genes related to the TES and endothelial cells, and constructed a risk model with four prognostic genes (*ALKBH2*, *TFPI2*, *PLAU*, and *CXCL8*). The model showed significant differences between high - and low-risk groups in immune cell infiltration, immune-related functions, and immune checkpoint expression. *CXCL8* was correlated with activated mast cells and CD276. The two risk groups responded differently to immunotherapies (anti - CTLA - 4 alone or with PD1/PDL1/PDL2) and drug treatments (e.g., axitinib). These findings indicate that the model can predict the survival of cervical cancer patients, aiding prognosis assessment and immunotherapy strategy development.

However, the study has limitations. It is a retrospective analysis lacking independent clinical validation, overly reliant on computational analysis with insufficient experimental verification, and the mechanisms of the prognostic genes in cervical cancer pathogenesis remain unclear. Future research should expand prospective cohort studies, conduct functional experiments to explore gene regulatory mechanisms, and integrate multi-omics technologies to enhance the model's clinical value and advance the precise treatment of CC.

Abbreviations

Abbreviation	Full Name
CC	Cervical cancer
TES	Tumor ecosystem
TCGA	The cancer genome atlas
GEO	Gene expression omnibus
DEGs	Differentially expressed genes
HRG	High-risk group
LRG	Low-risk group
HPV	Human papillomavirus
QoL	Quality of life
TES	Tumor ecosystem
TECs	Tumor-derived endothelial cells
NECs	Normal endothelial cells
DEGs	Differentially expressed genes
scRNA-seq	Single-cell rna sequencing
TME	Tumor microenvironment
FC	Fold-change
PCA	Principal component analysis
HR	Hazard ratio
PH	Proportional hazards
LASSO	Least absolute shrinkage and selection operator
K-M	Kaplan-meier

ROC	Receiver operating characteristic	402
GSVA	Gene set variation analysis	
IPS	Immunophenotype scores	
RT-qPCR	Reverse transcription-quantitative polymerase chain reaction	
cDNA	Complementary DNA	
GO	Gene ontology	
BPs	Biological processes	
CCs	Cellular components	
MFs	Molecular functions	
KEGG	Kyoto encyclopedia of genes and genomes	
AUC	Area under the curve	
EMT	Epithelial-mesenchymal transition	
CSCs	Cancer stem cells	
HNSCC	Head and neck squamous cell carcinoma	
EC	Endothelial cells	

403 **Funding**

404 This work was supported by [Yunnan revitalization talent support program] (Grant numbers [XDYC-YLWS-2024-
405 0079])and [Beijing Science and Technology Medical Development Foundation](Grant numbers [KC2023-JX-0288-
406 BZ15]) : The authors did not receive support from any organization for the submitted work.

407 **Conflicts of interest**

408 The authors have no relevant financial or non-financial interests to disclose.

409 **Ethis approval**

410 All procedures performed in studies involving human participants were in accordance with the ethical standards of the
411 institutional and/or national research committee and with the 1964 Helsinki Declaration and its later amendments or
412 comparable ethical standards. The study was approved by the clinical research ethics committee of Yunnan First People's
413 Hospital (NO. 2025-04-01/KHLL2025-KY101)

414 **Consent to participate**

Informed consent was obtained from all individual participants included in the study.

Data availability statements

The datasets generated during and/or analysed during the current study are available in the GEO database (https://www.ncbi.nlm.nih.gov/geo/) in GSE63514 and GSE9750, the Cancer Genome Atla (https://www.cancer.gov/ccg/research/genome-sequencing/tcga)

Reference

[1] Sung H, Ferlay J, Siegel RL, Laversanne M, Soerjomataram I, Jemal A, et al. Global Cancer Statistics 2020: GLOBOCAN Estimates of Incidence and Mortality Worldwide for 36 Cancers in 185 Countries. CA Cancer J Clin 2021; 71: 209-49. https://doi.org/10.3322/caac.21660

[2] Johnson CA, James D, Marzan A, and Armaos M. Cervical Cancer: An Overview of Pathophysiology and Management. Semin Oncol Nurs 2019; 35: 166-74. https://doi.org/10.1016/j.soncn.2019.02.003

[3] Xing X, Tian Y, and Jin X. Immune infiltration and a necroptosis-related gene signature for predicting the prognosis of patients with cervical cancer. Front Genet 2022; 13: 1061107. https://doi.org/10.3389/fgene.2022.1061107

[4] Yang X, Yin F, Liu Q, Ma Y, Zhang H, Guo P, et al. Ferroptosis-related genes identify tumor immune microenvironment characterization for the prediction of prognosis in cervical cancer. Ann Transl Med 2022; 10: 123. https://doi.org/10.21037/atm-21-6265

[5] Sedlis A, Bundy BN, Rotman MZ, Lentz SS, Muderspach LI, and Zaino RJ. A randomized trial of pelvic radiation therapy versus no further therapy in selected patients with stage IB carcinoma of the cervix after radical hysterectomy and pelvic lymphadenectomy: A Gynecologic Oncology Group Study. Gynecol Oncol 1999; 73: 177-83. https://doi.org/10.1006/gyno.1999.5387

[6] Moore, and DH. Cervical cancer. Obstetrics & Gynecology 2006; 107: 1152-61. https://doi.org/10.1097/01.AOG.0000215986.48590.79.

[7] Monk BJ, Huang HQ, Cella D, et al. Quality of Life Outcomes From a Randomized Phase III Trial of Cisplatin With or Without Topotecan in Advanced Carcinoma of the Cervix: A Gynecologic Oncology Group Study. J lin oncol. 2005; 23: 4617-25. https://doi.org/10.1200/JCO.2005.10.522.

[8] Ma L, Hernandez MO, Zhao Y, Mehta M, and Wang XWJCC. Tumor Cell Biodiversity Drives Microenvironmental Reprogramming in Liver Cancer. 2019; 36: 418-430.e6. https://doi.org/10.1016/j.ccell.2019.08.007. Epub 2019 Oct 3.

[9] Wu R, Gao Y, Zhao X, Guo S, Zhou H, Zhang Y, et al. Tumor biology, immune infiltration and liver function define seven hepatocellular carcinoma subtypes linked to distinct drivers, survival and drug response. Computers in biology and medicine 2023; 167: 107593. https://doi.org/10.1016/j.compbiomed.2023.107593

[10] Gong Y, Bao L, Xu T, Yi X, Chen J, Wang S, et al. The tumor ecosystem in head and neck squamous cell carcinoma and advances in ecotherapy. Molecular cancer 2023; 22: 68. https://doi.org/10.1186/s12943-023-01769-z

[11] Hida K, Kawamoto T, Ohga N, Akiyama K, Hida Y, and Shindoh M. Altered angiogenesis in the tumor microenvironment. Pathology international 2011; 61: 630-7. https://doi.org/10.1111/j.1440-1827.2011.02726.x

[12] Li C, Guo L, Li S, and Hua K. Single-cell transcriptomics reveals the landscape of intra-tumoral heterogeneity and transcriptional activities of ECs in CC. Molecular therapy. Nucleic acids 2021; 24: 682-94. https://doi.org/10.1016/j.omtn.2021.03.017

[13] Stuart T, Butler A, Hoffman P, Hafemeister C, Papalexi E, Mauck WM, 3rd, et al. Comprehensive Integration of Single-Cell Data. Cell 2019; 177: 1888-1902.e21. https://doi.org/10.1016/j.cell.2019.05.031

[14] Zhang Y, Wang D, Peng M, Tang L, Ouyang J, Xiong F, et al. Single-cell RNA sequencing in cancer research. Journal of experimental & clinical cancer research : CR 2021; 40: 81. https://doi.org/10.1186/s13046-021-01874-1

[15] Zhang J, Li Z, Chen Z, Shi W, Xu Y, Huang Z, et al. Comprehensive analysis of macrophage-related genes in prostate cancer by integrated analysis of single-cell and bulk RNA sequencing. Aging 2024; 16: 6809-38. https://doi.org/10.18632/aging.205727

[16] Li C, Wu H, Guo L, Liu D, Yang S, Li S, et al. Single-cell transcriptomics reveals cellular heterogeneity and molecular stratification of cervical cancer. Communications biology 2022; 5: 1208. https://doi.org/10.1038/s42003-022-04142-w

[17] Li C, Liu D, Yang S, and Hua K. Integrated single-cell transcriptome analysis of the tumor ecosystems underlying cervical cancer metastasis. Frontiers in immunology 2022; 13: 966291. https://doi.org/10.3389/fimmu.2022.966291

[18] Ritchie ME, Phipson B, Wu D, Hu Y, Law CW, Shi W, et al. limma powers differential expression analyses for RNA-sequencing and microarray studies. Nucleic acids research 2015; 43: e47. https://doi.org/10.1093/nar/gkv007

[19] Gustavsson EK, Zhang D, Reynolds RH, Garcia-Ruiz S, and Ryten M. ggtranscript: an R package for the visualization and interpretation of transcript isoforms using ggplot2. Bioinformatics 2022; 38: 3844-6. https://doi.org/10.1093/bioinformatics/btac409

[20] Gu Z, Eils R, and Schlesner M. Complex heatmaps reveal patterns and correlations in multidimensional genomic data. Bioinformatics (Oxford, England) 2016; 32: 2847-9. https://doi.org/10.1093/bioinformatics/btw313

[21] Hao Y, Hao S, Andersen-Nissen E, Mauck WM, 3rd, Zheng S, Butler A, et al. Integrated analysis of multimodal single-cell data. Cell 2021; 184: 3573-3587.e29. https://doi.org/10.1016/j.cell.2021.04.048

[22] Chen ZP, Wang S, Zhao X, Fang W, Wang Z, Ye H, et al. Lipid-accumulated reactive astrocytes promote disease progression in epilepsy. Nature neuroscience 2023; 26: 542-54. https://doi.org/10.1038/s41593-023-01288-6

[23] Liu C, Zhang M, Yan X, Ni Y, Gong Y, Wang C, et al. Single-cell dissection of cellular and molecular features underlying human cervical squamous cell carcinoma initiation and progression. Science advances 2023; 9: eadd8977. https://doi.org/10.1126/sciadv.add8977

[24] Griss J, Viteri G, Sidiropoulos K, Nguyen V, Fabregat A, and Hermjakob H. ReactomeGSA - Efficient Multi-Omics Comparative Pathway Analysis. Molecular & cellular proteomics : MCP 2020; 19: 2115-25. https://doi.org/10.1074/mcp.TIR120.002155

[25] Chen H, and Boutros PC. VennDiagram: a package for the generation of highly-customizable Venn and Euler diagrams in R. BMC bioinformatics 2011; 12: 35. https://doi.org/10.1186/1471-2105-12-35

[26] Lei J, Qu T, Cha L, Tian L, Qiu F, Guo W, et al. Clinicopathological characteristics of pheochromocytoma/paraganglioma and screening of prognostic markers. Journal of surgical oncology 2023; 128: 510-8. https://doi.org/10.1002/jso.27358

[27] Engebretsen S, and Bohlin J. Statistical predictions with glmnet. Clinical epigenetics 2019; 11: 123. https://doi.org/10.1186/s13148-019-0730-1

[28] Liu TT, Li R, Huo C, Li JP, Yao J, Ji XL, et al. Identification of CDK2-Related Immune Forecast Model and ceRNA in Lung Adenocarcinoma, a Pan-Cancer Analysis. Frontiers in cell and developmental biology 2021; 9: 682002. https://doi.org/10.3389/fcell.2021.682002

[29] Heagerty PJ, Lumley T, and Pepe MS. Time-dependent ROC curves for censored survival data and a diagnostic marker. Biometrics 2000; 56: 337-44. https://doi.org/10.1111/j.0006-341x.2000.00337.x

[30] Xu J, Yang T, Wu F, Chen T, Wang A, and Hou S. A nomogram for predicting prognosis of patients with cervical cerclage. Heliyon 2023; 9: e21147. https://doi.org/10.1016/j.heliyon.2023.e21147

[31] Ashwell KW, and Zhang LL. Ontogeny of afferents to the fetal rat cerebellum. Acta anatomica 1992; 145: 17-23. https://doi.org/10.1159/000147336

[32] Hänzelmann S, Castelo R, and Guinney J. GSVA: gene set variation analysis for microarray and RNA-seq data. BMC bioinformatics 2013; 14: 7. https://doi.org/10.1186/1471-2105-14-7

[33] Chen X, Zhang Z, Qin Z, Zhu X, Wang K, Kang L, et al. Identification and validation of a novel signature based on macrophage marker genes for predicting prognosis and drug response in kidney renal clear cell carcinoma by integrated analysis of single cell and bulk RNA sequencing. Aging 2024; 16: 5676-702. https://doi.org/10.18632/aging.205671

[34] Robles-Jimenez LE, Aranda-Aguirre E, Castelan-Ortega OA, Shettino-Bermudez BS, Ortiz-Salinas R, Miranda M, et al. Worldwide Traceability of Antibiotic Residues from Livestock in Wastewater and Soil: A Systematic Review. Animals : an open access journal from MDPI 2021; 12: 60. https://doi.org/10.3390/ani12010060

[35] Efremova M, Vento-Tormo M, Teichmann SA, and Vento-Tormo R. CellPhoneDB: inferring cell-cell communication from combined expression of multi-subunit ligand-receptor complexes. Nature protocols 2020; 15: 1484-506. https://doi.org/10.1038/s41596-020-0292-x

[36] Geeleher P, Cox N, and Huang RS. pRRophetic: an R package for prediction of clinical chemotherapeutic response from tumor gene expression levels. PLoS One 2014; 9: e107468. https://doi.org/10.1371/journal.pone.0107468

[37] Hu MD, Jia LH, and Wang ML. PLAU contributes to the development of cholangiocarcinoma via activating NF-κB signaling pathway. Cell biology international 2023; 47: 1381-91. https://doi.org/10.1002/cbin.12025

[38] Shi K, Zhou J, Li M, Yan W, Zhang J, Zhang X, et al. Pan-cancer analysis of PLAU indicates its potential prognostic value and correlation with neutrophil infiltration in BLCA. Biochimica et biophysica acta. Molecular basis of disease 2024; 1870: 166965. https://doi.org/10.1016/j.bbadis.2023.166965

[39] Li Z, Chen C, Wang J, Wei M, Liu G, Qin Y, et al. Overexpressed PLAU and its potential prognostic value in head and neck squamous cell carcinoma. PeerJ 2021; 9: e10746. https://doi.org/10.7717/peerj.10746

[40] Li D, Ding C, Huang F, Chang M, Lu Z, Li G, et al. Bioinformatics Analysis of the Expression and Prognostic Value of PLAU Gene in Wilms' Tumor. Anticancer research 2024; 44: 3829-42. https://doi.org/10.21873/anticanres.17209

[41] Gao Y, Ma X, Lu H, Xu P, and Xu C. PLAU is associated with cell migration and invasion and is regulated by transcription factor YY1 in cervical cancer. Oncology reports 2023; 49: 25. https://doi.org/10.3892/or.2022.8462

[42] Zhang N, Pang C, Li Z, Xu F, and Zhao L. Serum CXCL8 and CXCR2 as diagnostic biomarkers for noninvasive screening of cervical cancer. Medicine 2023; 102: e34977. https://doi.org/10.1097/md.0000000000034977

[43] Zhang X, Yang J, Feng Q, Gu L, Qin G, Cheng C, et al. The immune landscape and prognostic analysis of CXCL8 immune-related genes in cervical squamous cell carcinoma. Environmental toxicology 2025; 40: 902-11. https://doi.org/10.1002/tox.24283

[44] Yan R, Shuai H, Luo X, Wang X, and Guan B. The clinical and prognostic value of CXCL8 in cervical carcinoma patients: immunohistochemical analysis. Bioscience reports 2017; 37: BSR20171021. https://doi.org/10.1042/bsr20171021

[45] Ribarska T, Ingenwerth M, Goering W, Engers R, and Schulz WA. Epigenetic inactivation of the placentally imprinted tumor suppressor gene TFPI2 in prostate carcinoma. Cancer genomics & proteomics 2010; 7: 51-60.

[46] Sato N, Parker AR, Fukushima N, Miyagi Y, Iacobuzio-Donahue CA, Eshleman JR, et al. Epigenetic inactivation of TFPI-2 as a common mechanism associated with growth and invasion of pancreatic ductal adenocarcinoma. Oncogene 2005; 24: 850-8. https://doi.org/10.1038/sj.onc.1208050

[47] Geng G, Liu X, Xu A, Lu Z, Chen K, He J, et al. Low abundance of TFPI-2 by both promoter methylation and miR-27a-3p regulation is linked with poor clinical outcome in gastric cancer. The journal of gene medicine 2020; 22: e3166. https://doi.org/10.1002/jgm.3166

[48] Hamamoto J, Soejima K, Naoki K, Yasuda H, Hayashi Y, Yoda S, et al. Methylation-induced downregulation of TFPI-2 causes TMPRSS4 overexpression and contributes to oncogenesis in a subset of non-small-cell lung carcinoma. Cancer science 2015; 106: 34-42. https://doi.org/10.1111/cas.12569

[49] Zhao D, Qiao J, He H, Song J, Zhao S, and Yu J. TFPI2 suppresses breast cancer progression through inhibiting TWIST-integrin α5 pathway. Molecular medicine (Cambridge, Mass.) 2020; 26: 27. https://doi.org/10.1186/s10020-020-00158-2

[50] Kremer V, Bink DI, Stanicek L, van Ingen E, Gimbel T, Hilderink S, et al. MEG8 regulates Tissue Factor Pathway Inhibitor 2 (TFPI2) expression in the endothelium. Scientific reports 2022; 12: 843. https://doi.org/10.1038/s41598-022-04812-z

[51] Fullár A, Karászi K, Hollósi P, Lendvai G, Oláh L, Reszegi A, et al. Two ways of epigenetic silencing of TFPI2 in cervical cancer. PloS one 2020; 15: e0234873. https://doi.org/10.1371/journal.pone.0234873

[52] Fujii T, Shimada K, Anai S, Fujimoto K, and Konishi N. ALKBH2, a novel AlkB homologue, contributes to human bladder cancer progression by regulating MUC1 expression. Cancer science 2013; 104: 321-7. https://doi.org/10.1111/cas.12089

[53] Wu G, Yan Y, Cai Y, Peng B, Li J, Huang J, et al. ALKBH1-8 and FTO: Potential Therapeutic Targets and Prognostic Biomarkers in Lung Adenocarcinoma Pathogenesis. Frontiers in cell and developmental biology 2021; 9: 633927. https://doi.org/10.3389/fcell.2021.633927

[54] Ke B, Ye K, and Cheng S. ALKBH2 inhibition alleviates malignancy in colorectal cancer by regulating BMI1-mediated activation of NF-κB pathway. World journal of surgical oncology 2020; 18: 328. https://doi.org/10.1186/s12957-020-02106-0

[55] Gui Z, Ye Y, Li Y, Ren Z, Wei N, Liu L, et al. Construction of a novel cancer-associated fibroblast-related signature to predict clinical outcome and immune response in cervical cancer. Translational oncology 2024; 46: 102001. https://doi.org/10.1016/j.tranon.2024.102001

[56] Wang M, and Li Z. Prediction of prognosis and immune landscape in cervical cancer based on heat shock protein-related genes. International journal of hyperthermia : the official journal of European Society for Hyperthermic Oncology, North American Hyperthermia Group 2023; 40: 2259140. https://doi.org/10.1080/02656736.2023.2259140

[57] Hart PH, Townley SL, Grimbaldeston MA, Khalil Z, and Finlay-Jones JJ. Mast cells, neuropeptides, histamine, and prostaglandins in UV-induced systemic immunosuppression. Methods (San Diego, Calif.) 2002; 28: 79-89. https://doi.org/10.1016/s1046-2023(02)00201-3

[58] Masini E, Fabbroni V, Giannini L, Vannacci A, Messerini L, Perna F, et al. Histamine and histidine decarboxylase up-regulation in colorectal cancer: correlation with tumor stage. Inflammation research : official journal of the European Histamine Research Society ... [et al.] 2005; 54 Suppl 1: S80-1. https://doi.org/10.1007/s00011-004-0437-3

[59] Cianchi F, Cortesini C, Perna F, Fabbroni V, Uliva C, Fabrizi F, et al. Prostaglandin E(2) correlates with histamine production in human colorectal cancer. Inflammation research : official journal of the European Histamine Research Society ... [et al.] 2006; 55 Suppl 1: S81-2. https://doi.org/10.1007/s00011-005-0053-x

[60] Rudolph MI, Boza Y, Yefi R, Luza S, Andrews E, Penissi A, et al. The influence of mast cell mediators on migration of SW756 cervical carcinoma cells. Journal of pharmacological sciences 2008; 106: 208-18. https://doi.org/10.1254/jphs.fp0070736

[61] Wang C, Li Y, Jia L, Kim JK, Li J, Deng P, et al. CD276 expression enables squamous cell carcinoma stem cells to evade immune surveillance. Cell stem cell 2021; 28: 1597-1613.e7. https://doi.org/10.1016/j.stem.2021.04.011

[62] Han S, Wang Y, Shi X, Zong L, Liu L, Zhang J, et al. Negative roles of B7-H3 and B7-H4 in the microenvironment of cervical cancer. Experimental cell research 2018; 371: 222-30. https://doi.org/10.1016/j.yexcr.2018.08.014

[63] Li Y, Zhang J, Han S, Qian Q, Chen Q, Liu L, et al. B7-H3 promotes the proliferation, migration and invasiveness of cervical cancer cells and is an indicator of poor prognosis. Oncology reports 2017; 38: 1043-50. https://doi.org/10.3892/or.2017.5730

[64] Michaelis UR. Mechanisms of endothelial cell migration. Cellular and molecular life sciences : CMLS 2014; 71: 4131-48. https://doi.org/10.1007/s00018-014-1678-0

[65] Wu X, Newbold MA, Gao Z, and Haynes CL. A versatile microfluidic platform for the study of cellular interactions between endothelial cells and neutrophils. Biochimica et biophysica acta. General subjects 2017; 1861: 1122-30. https://doi.org/10.1016/j.bbagen.2017.02.012

[66] Tsumita T, Maishi N, Annan DA, Towfik MA, Matsuda A, Onodera Y, et al. The oxidized-LDL/LOX-1 axis in tumor endothelial cells enhances metastasis by recruiting neutrophils and cancer cells. International journal of cancer 2022; 151: 944-56. https://doi.org/10.1002/ijc.34134

Table 1: Differences in different cell types between disease and control groups

celltype	pvalue
Epithelial/cancer cells	0
Endothelial cells	0
Smooth muscle cells	0
Fibroblasts	0
T cells	6.19E-187
Neutrophils	9.46E-147
Macrophage	2.39E-16
B cells	6.31E-22

Table 2: PH test results

	chisq	df	p
CXCL1	2.04505053006097	1	0.152701913801918
PLAU	0.0559474930166832	1	0.813019705375833
CXCL8	1.14164640363828	1	0.285304702790106
ALKBH2	2.38879623546045	1	0.122207699765824
TFPI2	0.237807978184313	1	0.625793810366948
ISG20	4.30386882305812	1	0.0380257758226724

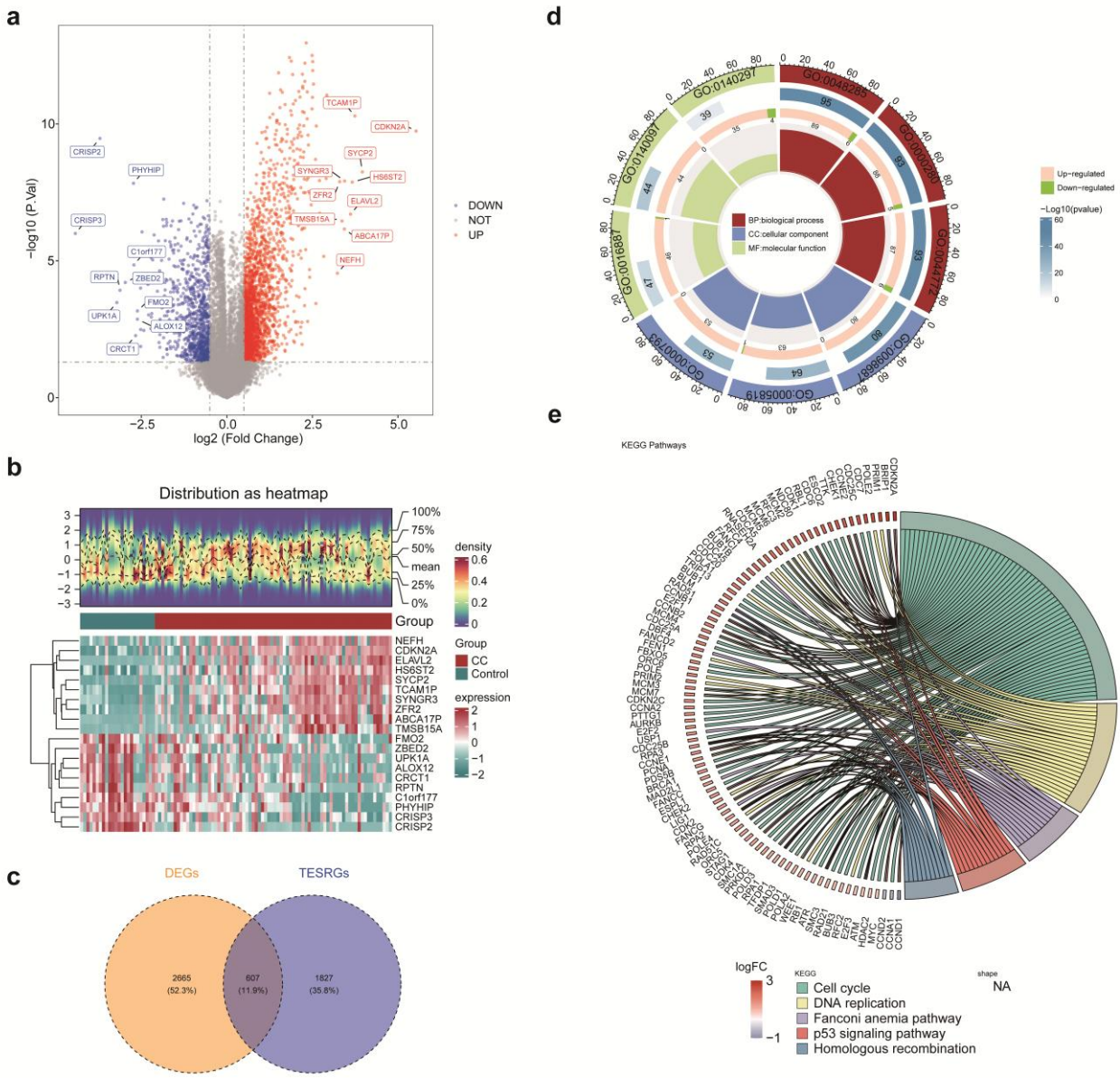


Fig1. Identification and functional enrichment analysis of differentially expressed genes (DEGs) associated with the tumor ecosystem (TES). (a) Volcano plot displaying DEGs between cervical cancer (CC) and control samples. **(b)** Heatmap of top 20 DEGs (10 up-regulated and 10 down-regulated) in CC. **(c)** Venn diagram showing the overlap between DEGs and TES-related genes (TES-RGs). **(d)** Bar plot of enriched Gene Ontology (GO) terms for DEGs associated with TES. **(e)** Bar plot of enriched Kyoto Encyclopedia of Genes and Genomes (KEGG) pathways for DEGs associated with TES.

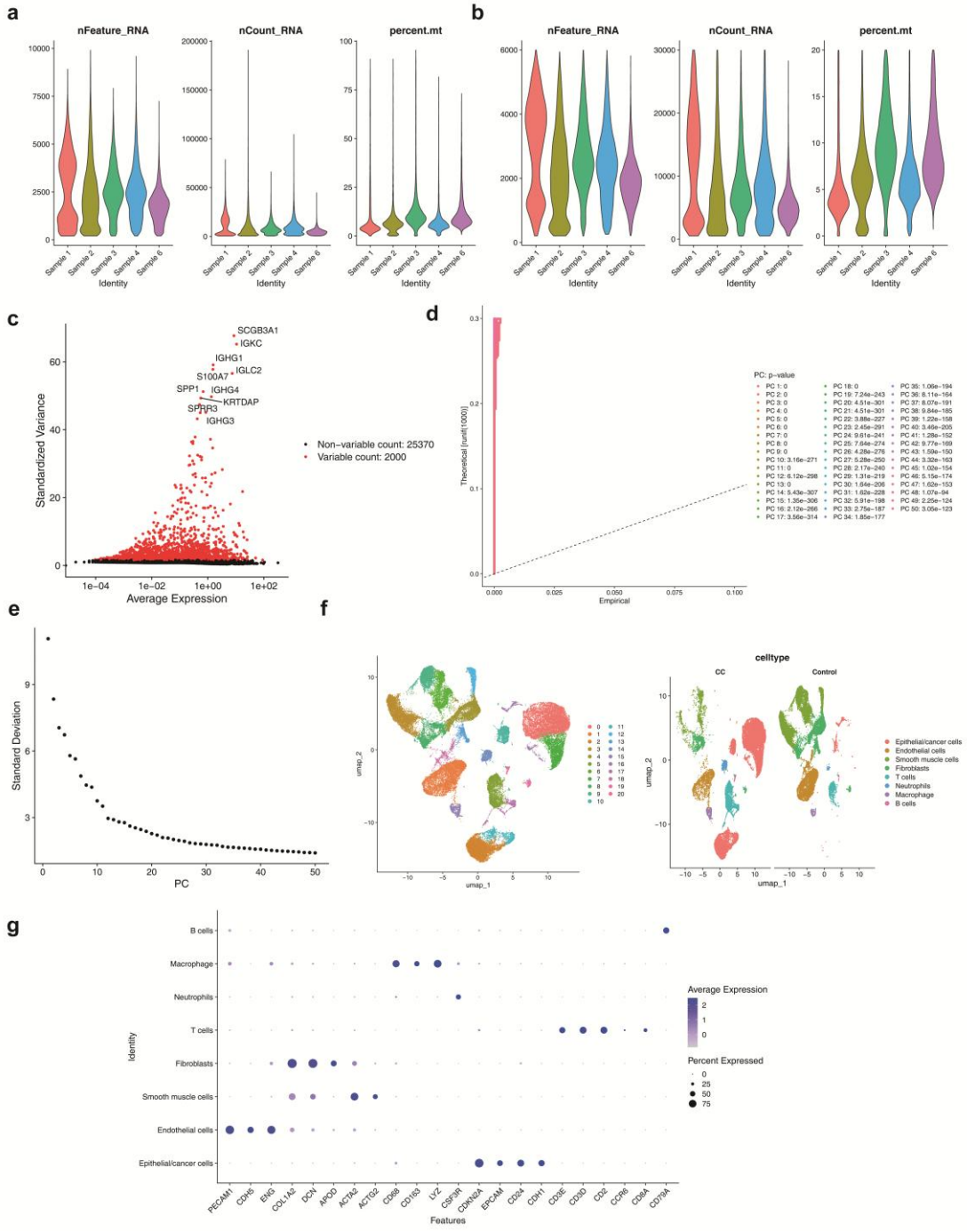


Fig2. Single-cell RNA sequencing (scRNA-seq) analysis of cervical cancer samples. (a) Distribution of gene counts per cell before quality control. **(b)** Distribution of gene counts per cell after quality control. **(c)** Scatter plot of highly variable genes, with top 10 genes labeled. **(d)** Principal component analysis (PCA) plot of scRNA-seq data. **(e)** Jackstraw plot for significant principal components. **(f)** UMAP plot showing unsupervised clustering of cells. **(g)** UMAP plot annotated by cell types. **(h)** Dot plot of marker genes for identified cell types.

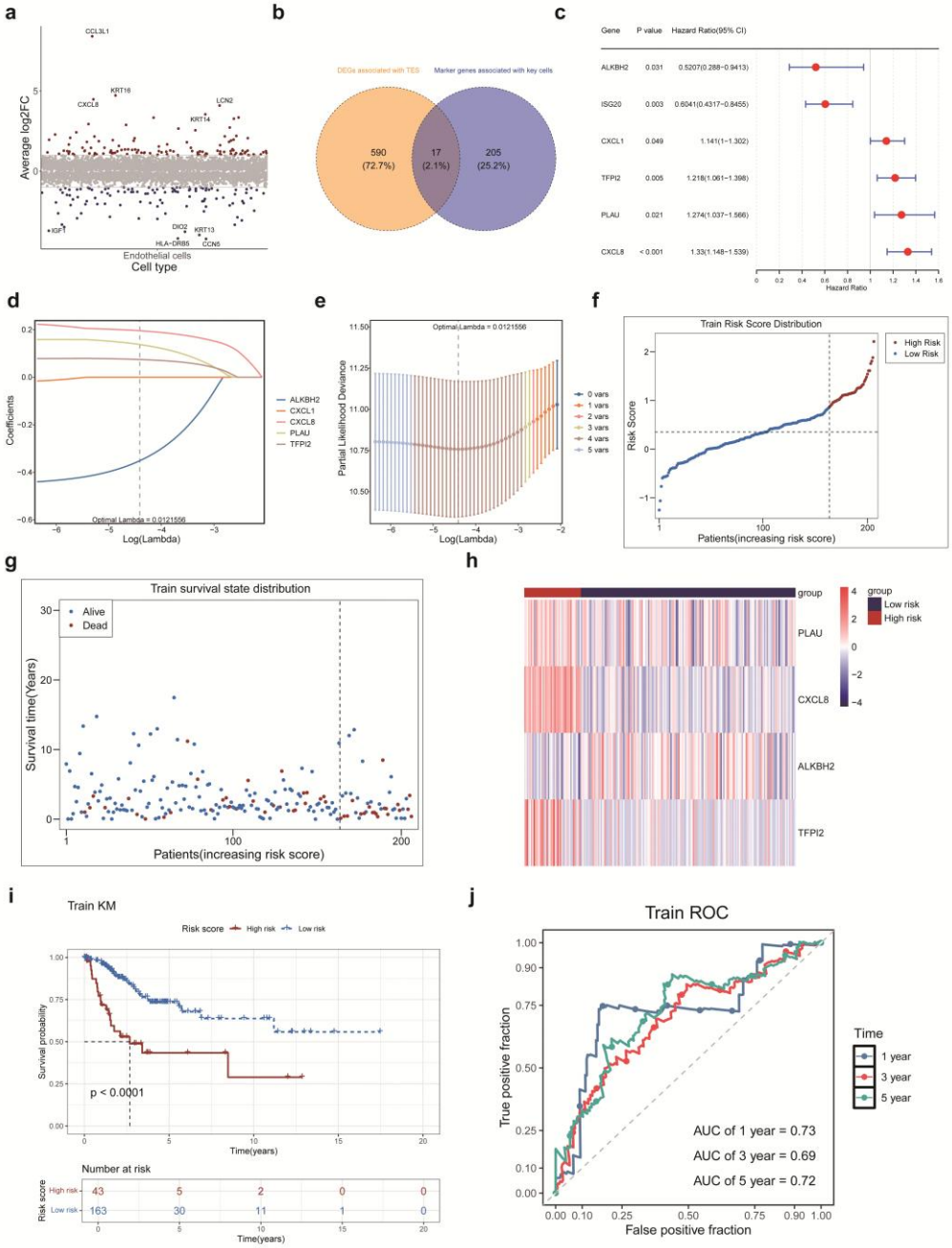


Fig3. Construction and validation of the risk model related to TES and endothelial cells. (a) Manhattan plot of differentially expressed genes in endothelial cells. **(b)** Venn diagram of candidate genes from DEGs associated with TES and endothelial cell markers. **(c)** Forest plot of univariate Cox regression analysis for candidate genes. **(d)** LASSO coefficient profiles of prognostic genes. **(e)** Cross-validation for selecting the optimal lambda value in LASSO regression. **(f)** Risk score distribution for samples in the training set. **(g)** Scatter plot of survival status versus risk score. **(h)** Heatmap of prognostic gene expression in high-risk (HRG) and low-risk (LRG) groups. **(i)** Kaplan-Meier survival curves for HRG and LRG. **(j)** Receiver operating characteristic (ROC) curves for 1-, 3-, and 5-year survival prediction.

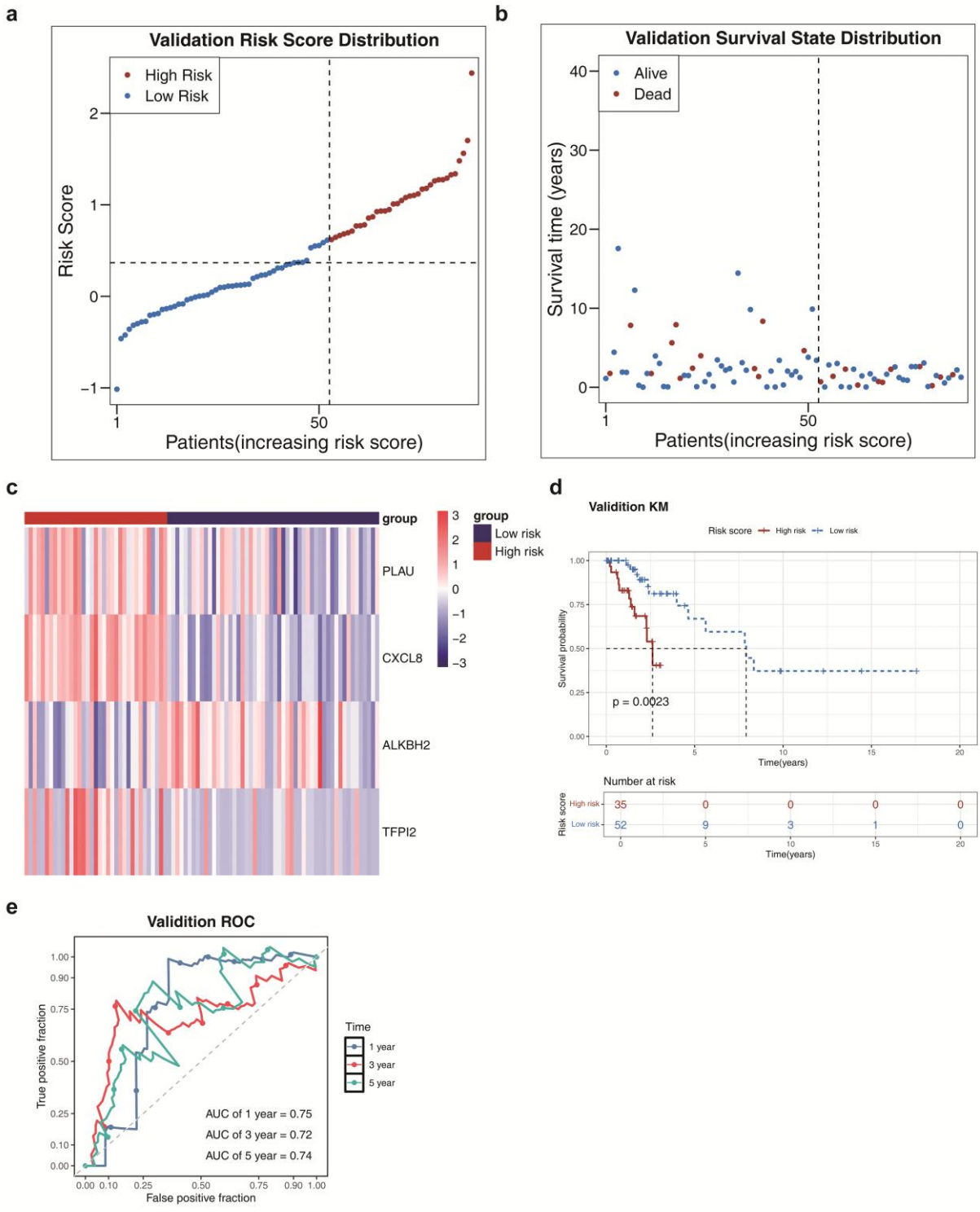


Fig4. Validation of the risk model in the independent dataset. (a) Risk score distribution for samples in the validation set. **(b)** Scatter plot of survival status versus risk score. **(c)** Heatmap of prognostic gene expression in HRG and LRG. **(d)** Kaplan-Meier survival curves for HRG and LRG. **(e)** ROC curves for 1-, 3-, and 5-year survival prediction.

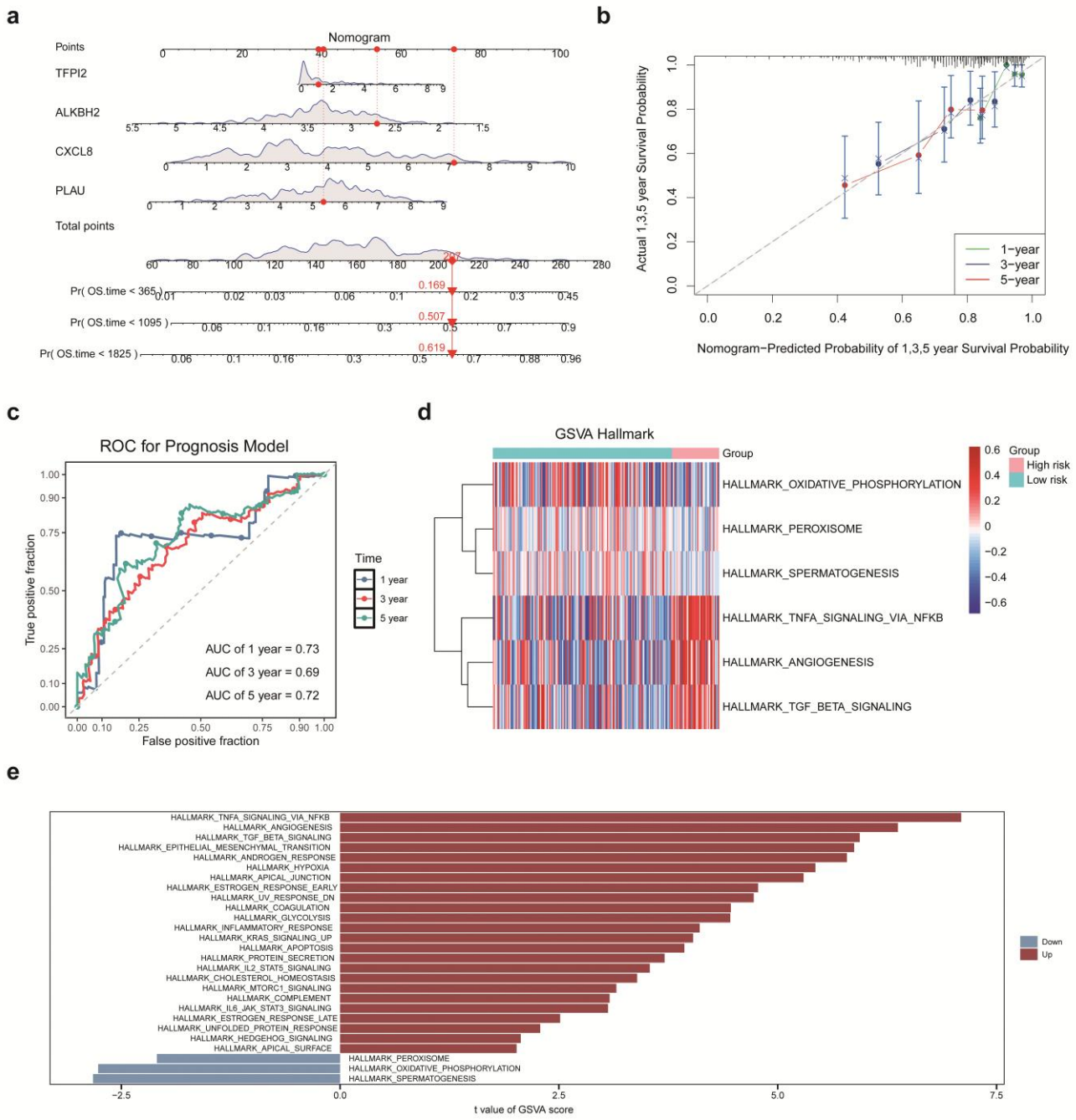


Fig5. Prognostic nomogram and enrichment analysis. (a) Nomogram for predicting overall survival in CC patients. **(b)** Calibration curve for the nomogram model. **(c)** ROC curves for the nomogram's predictive performance. **(d)** Heatmap of differentially enriched pathways between HRG and LRG. **(e)** Bar plot of significantly activated or suppressed pathways in HRG.

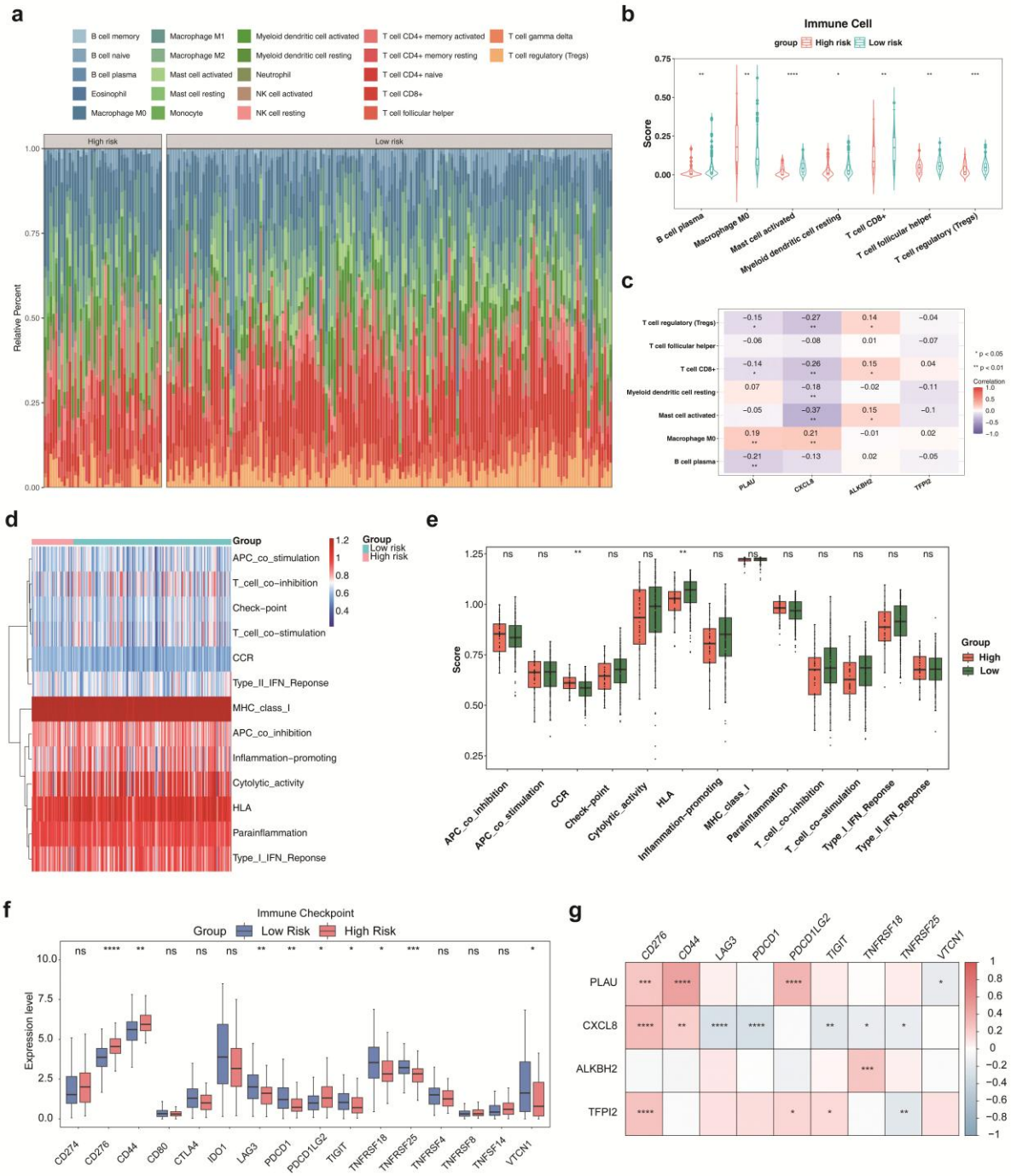


Fig6. Immune infiltration landscape in HRG and LRG. (a) Heatmap of immune cell infiltration scores. **(b)** Box plots of differentially infiltrated immune cells. **(c)** Correlation heatmap between prognostic genes and immune cells. **(d)** Heatmap of immune-related functions. **(e)** Box plots of differentially expressed immune-related functions. **(f)** Box plots of differentially expressed immune checkpoints. **(g)** Correlation heatmap between prognostic genes and immune checkpoints.

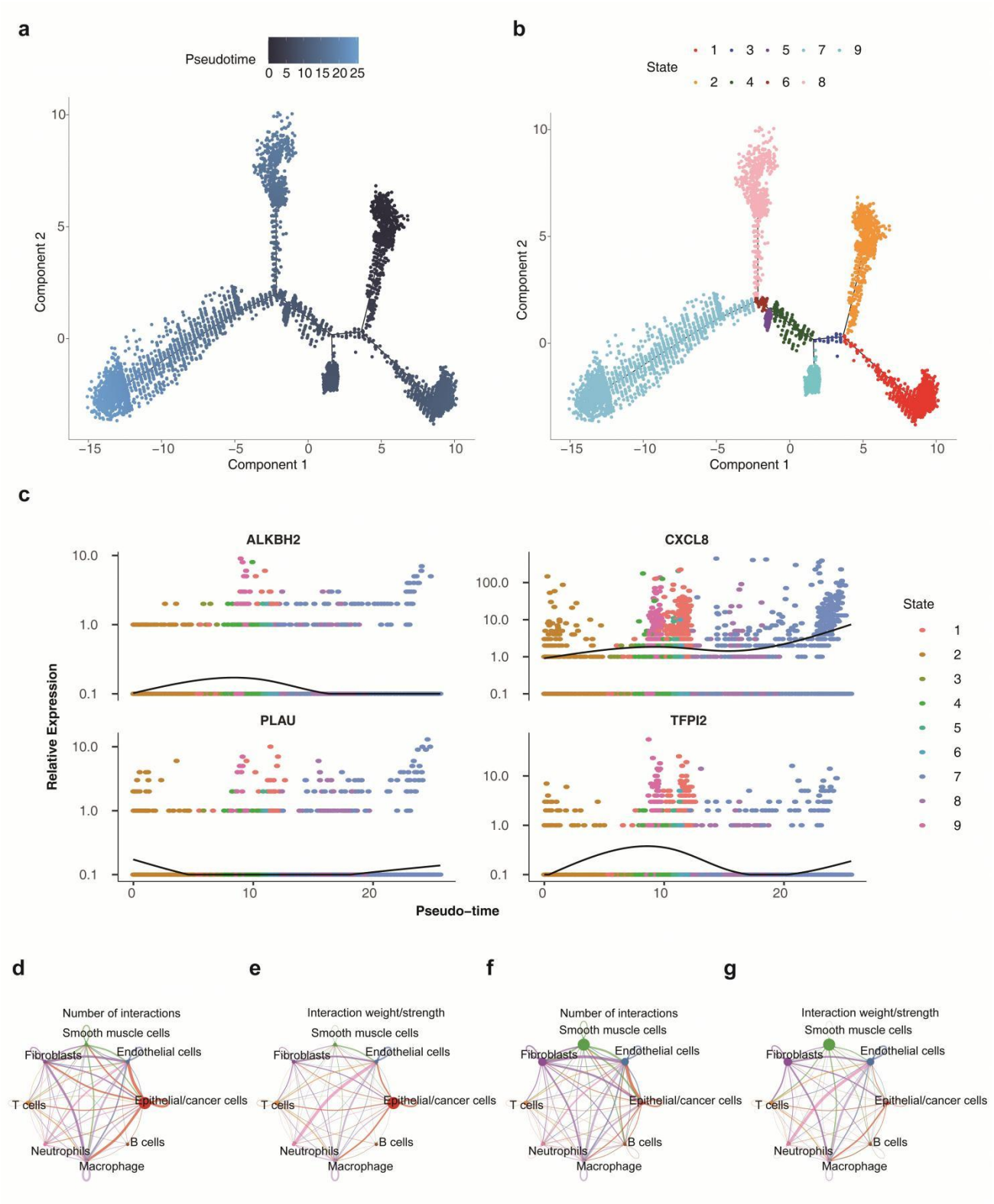


Fig7. Evolutionary trajectory and cellular communication analysis of endothelial cells. (a) UMAP plot showing endothelial cell subgroups. **(b)** Pseudotime trajectory of endothelial cell development. **(c)** Line plots showing expression trends of prognostic genes along pseudotime. **(d)** Cell-cell interaction network in control samples. **(e)** Interaction strength

between endothelial cells and other cell types in control samples. **(f)** Cell-cell interaction network in CC samples. **(G)** Interaction strength between endothelial cells and other cell types in CC samples.

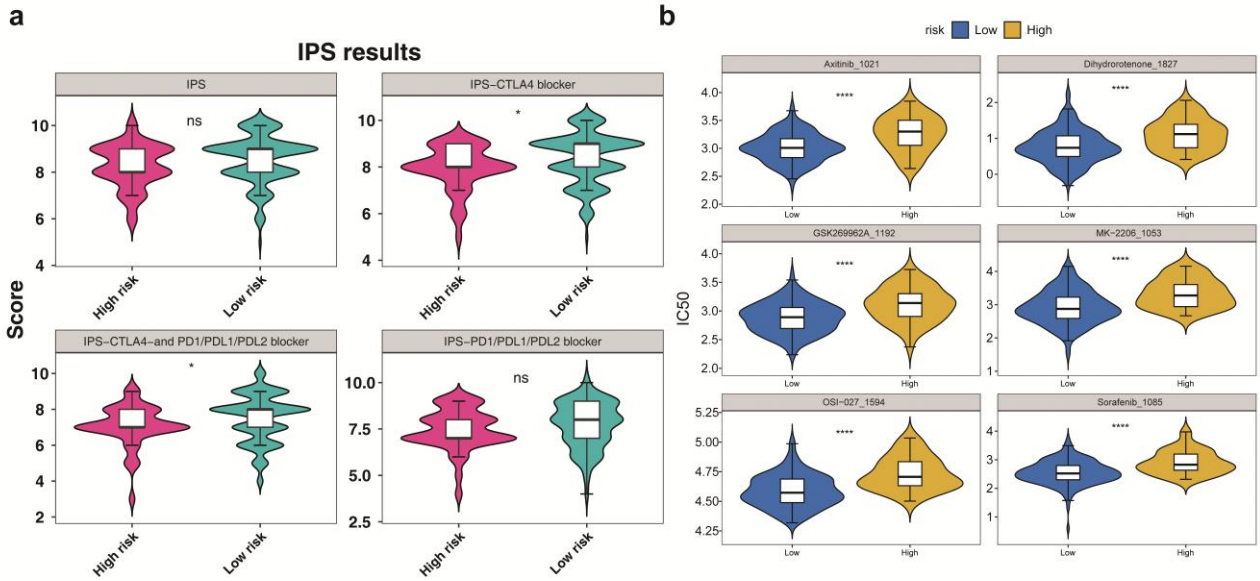
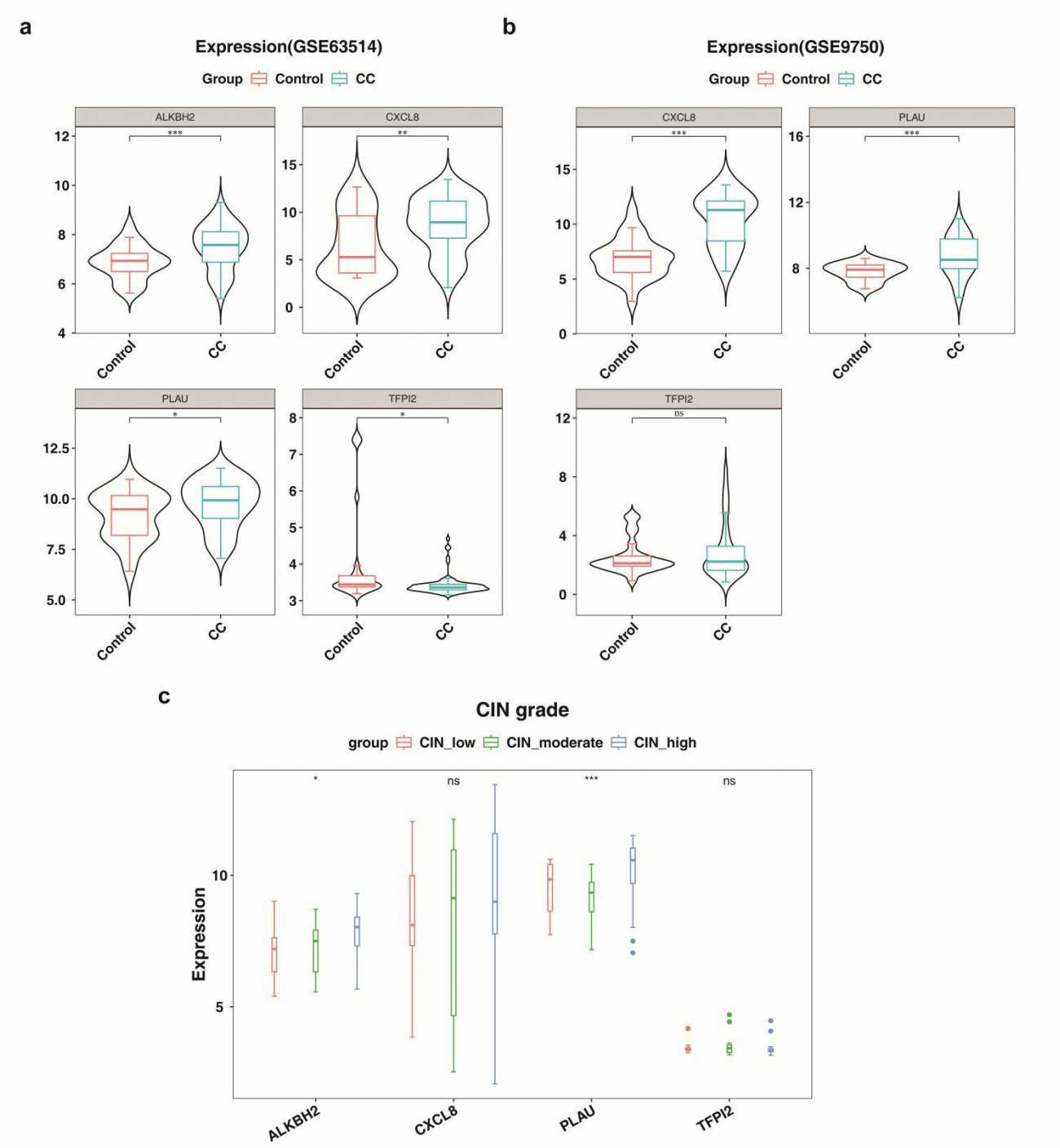


Fig8. Immunotherapy and drug sensitivity analysis. (a) Box plots of immunophenotype scores (IPS) for HRG and LRG under different immunotherapy regimens. **(b)** Heatmap of drug sensitivity differences between HRG and LRG.



689

690 **Fig9. Expression validation of prognostic genes. (a)** Box plots of prognostic gene expression in GSE63514 dataset. **(b)**

691 Box plots of prognostic gene expression in GSE9750 dataset. **(c)** Box plots of prognostic gene expression across different

692 tumor grades. **(d)** Bar plot of RT-qPCR results for prognostic genes in clinical samples.

693

694

695

Supplementary Information

Online Resource 1 Primer sequences for RT-qPCR validation of prognostic genes

Online Resource 2 GO enrichment analysis results of DEGs associated with TES

Online Resource 3 KEGG enrichment analysis results of DEGs associated with TES

Online Resource 4 Functional enrichment of cell types identified by scRNA-seq.

Online Resource 5 Functional enrichment analysis of cell types identified by scRNA-seq

Online Resource 6 Correlation between prognostic genes and immune checkpoints (Spearman test)

Online Resource 7 TIMER algorithm: Immune cell infiltration differences between HRG and LRG.

Online Resource 8 TIMER algorithm: Correlation matrix of immune cell infiltration.

Online Resource 9 TIMER algorithm: Prognostic genes vs. immune cell infiltration.

Online Resource 10 TIMER algorithm: Correlation between prognostic genes and immune cell infiltrationSupplementary Figures and Tables

Online Resource 11 XCELL algorithm: Immune cell infiltration differences.

Online Resource 12 XCELL algorithm: Immune cell infiltration heatmap.

Online Resource 13 XCELL algorithm: Prognostic genes vs. immune cell correlation.

Online Resource 14 Summary table XCELL algorithm: Prognostic genes vs. immune cell correlation.

Supplementary Files

This is a list of supplementary files associated with this preprint. Click to download.

- OnlineResource6.xlsx
- OnlineResource1.xlsx
- OnlineResource10.xlsx
- OnlineResource14.xlsx
- OnlineResource3.xlsx
- OnlineResource2.xlsx
- OnlineResource5.xlsx
- OnlineResource8.tif
- OnlineResource12.tif
- OnlineResource9.tif
- OnlineResource13.tif
- OnlineResource4.tif
- OnlineResource11.tif
- OnlineResource7.tif